Damage estimate in high cycle fatigue by energy balance

Bruno Berthel [a], André Chrysochoos [a] , Bertrand Wattrisse [a] , Bastien Weber[b] and André Galtier

[a] Lab. of Mechanics and Civil Engineering,
CC 048, Pl. E. Bataillon, 34095 Montpellier, France
[b] Arcelor Research SA,
Voie Romaine BP 30320, 57283 Maizières-lès-Metz, France

Abstract This paper presents an experimental protocol developed to locally estimate different terms of the energy balance associated with the fatigue of DP 600 steel. The method involves two quantitative imaging techniques. First, digital image correlation (DIC) provides displacement fields and, after derivation, strain and strain rate fields. A method, based on the integration of the local equilibrium equations is used to estimate the stress fields. The deformation energy rate distribution can then be determined on the basis of the stress and strain data. Secondly, infrared thermography (IRT) provides thermal images which are used to separately estimate the thermoelastic source amplitude and mean dissipation per cycle distributions. The image processing uses a local form of the heat diffusion equation and a special set of approximation functions that take the frequency spectra of the sought sources into account.

1 INTRODUCTION

Characterization of fatigue in materials and mechanical components requires time-consuming and expensive statistical processing of the results of numerous mechanical tests. Alternative experimental approaches have been developed for several years to provide reliable fatigue characteristics more rapidly. Among these, the thermal methods, based on the analysis of the self-heating during a stepwise loading fatigue test, must be mentioned. This type of method appeared at the beginning of the 20th century [1] but its application really expanded these last twenty years [2-5]. In the references mentioned above, several authors claimed that the remarkable change in heating regime that occurs within a certain stress range is empirically related to the fatigue limit of the material. Although realistic estimates of this limit were sometimes obtained, the thermal approaches often led to questionable results [6-7]. Indeed, the physical implications of the threshold stress evaluated by these thermal methods are not well understood yet. In [7], it was shown that, starting from thermal response to cyclic loading, it is impossible to estimate the fatigue limit for a large number of steel grades, but it is just possible to determine a threshold of localization of plastic deformation. This threshold corresponds to the onset of persistent slip bands which number increased with stress.

In previous works we also underlined that the direct use of the specimen temperature as fatigue indicator is not always reliable because the temperature variation is not intrinsic to the material behaviour [8]. It depends actually on the diffusion properties (material effect) but also on thermal boundary conditions and on the distribution of heat sources (structure effects). In 1933, Taylor and Quinney have already seen the advantages of a calorimetric analysis of phenomena accompanying the deformation of the materials during monotonous tests [9]. Publications on the calorimetric analyses during fatigue test are not so numerous. Nevertheless, we can mention some papers like [10] in which energy balances at the specimen scale during low cycle fatigue (large plastic strain) are proposed. In [11] a method is derived concerning the rapid determination of the fatigue limit based on the dissipative measurement. In [12] energy balances at the specimen scale during high and low cycle fatigue are presented. Finally, in [13] 2D patterns of mean dissipation per cycle during a fatigue crack on a notched specimen are shown. Except for [13], these previous works are global energy approaches of the fatigue phenomena (i.e. at the specimen scale). Here we therefore studied fatigue phenomena using a local energy approach with the aim of experimentally determining the distributions of deformation energy rate and various heat sources accompanying the fatigue test in the high cycle fatigue domain. Speckle image correlation techniques, involving a digital CCD camera [14], were used to assess surface displacement fields. These kinematic fields enabled us to identify distributions stress patterns via an integration of the linear momentum equation. A local form of the heat equation was also used to derive heat sources from thermal images provided by an infrared camera. A specific thermal image processing method was therefore developed to estimate separately dissipated energy and thermoelastic coupling sources.

In what follows, we first review the expression of the different terms of the energy balance associated with high cycle fatigue of steels. We then briefly review kinematic and thermal image processing principles and the benefits of their combined use. Finally, preliminary results obtained on a dual-phase steel are presented to highlight the promising potential of this local energy approach.

2 LOCAL FORM OF THE ENERGY BALANCE

From a thermomechanical standpoint, fatigue is considered as a dissipative quasi-static process. Within the generalized standard materials framework [15], the equilibrium state of each volume material element is then described using a set of N state variables. The chosen variables are: the absolute temperature T, the linearized strain tensor ε (hypothesis of small perturbations) and N-2 scalar components α_1, α_2, …, α_{N-2} of vector α which pools the so-called internal variables. These latter variables describe the macroscopic effects of complex coupled microstructural phenomena. By construction, the thermodynamic potential is the Helmholtz free energy ψ.

The intrinsic dissipation d_1 is classically defined by:

$$d_1 = \left(\sigma - \rho \frac{\partial \psi}{\partial \varepsilon} \right) : \dot{\varepsilon} - \rho \frac{\partial \psi}{\partial \alpha} . \dot{\alpha} \tag{1}$$

where σ is the Cauchy stress tensor, ρ the mass density and C the specific heat.

The intrinsic dissipation d_1 is the difference between the rate of deformation energy

$$w^{\bullet}_{\text{def}} = \sigma : \dot{\varepsilon} \tag{2}$$

and the sum of elastic and stored energy-rates

$$w^{\bullet}_{\text{e}} + w^{\bullet}_{\text{s}} = \rho \frac{\partial \psi}{\partial \varepsilon} : \dot{\varepsilon} + \rho \frac{\partial \psi}{\partial \alpha} . \dot{\alpha} \tag{3}$$

The symbol $(\ )^{\bullet}$ means that the time variation of $(\ )$ is path-dependent.

To complete the energy balance, two others equations are needed. The first is given by first principle of thermodynamics:

$$\rho \dot{e} = \rho C \dot{T} + w^{\bullet}_{\text{e}} + w^{\bullet}_{\text{s}} - s_{the} - s_{ic} \tag{4}$$

where e is the specific internal energy, s_{the} and s_{ic} are respectively the thermoelastic and the internal coupling sources. With the specific free energy $\psi(T, \varepsilon, \alpha)$, the volume heat sources s_{the} and s_{ic} can be rewritten as:

$$\begin{cases} s_{\text{the}} = \rho T \dfrac{\partial^2 \psi}{\partial T \partial \varepsilon} : \dot{\varepsilon} \\ s_{\text{ic}} = \rho T \dfrac{\partial^2 \psi}{\partial T \partial \alpha} . \dot{\alpha} \end{cases} \tag{5}$$

The second, the local heat diffusion equation, is provided by combining both first and second principles of thermodynamics:

$$\rho C\dot{T} - \mathrm{div}(K\,\mathrm{grad}T) = d_1 + s_{\mathrm{the}} + s_{\mathrm{ic}} + r_{\mathrm{ext}} \tag{6}$$

where K is the conduction tensor and r_{ext} the external volume heat supply r_{ext}.

In the framework of our fatigue tests, temperature variations remained low and could not modify the internal state of the material, so we neglected the corresponding heat sources s_{ic} and the thermoelastic sources were computed via the classical linear thermoelastic model applied to uniaxial loadings. The thermoelastic source could then be written as $s_{\mathrm{the}} \approx -\alpha_{\mathrm{d}} T_0 \dot{\sigma}$, where α_{d} is the linear thermal expansion coefficient.

3 DIC & IRT IMAGE PROCESSING

3.1 Estimate of deformation energy rate

DIC gives the space-time patterns of various kinematic variables on the sample surface [14] (displacement, velocity, strain, strain-rate, acceleration, etc.). In our study, the image processing was systematically performed after the test in two steps. First, the displacement field was estimated. Secondly, the strains (or the strain-rates) were derived from the displacements by space (and time) differentiation. Each computational step involved a specific numerical processing procedure based on local least squares fitting, as thoroughly presented in [14]. The image processing performances were tested both on analytic and experimental cases corresponding to rigid body motion (translation or rotation), or to homogeneous or heterogeneous strain. In the case of fatigue tests described hereafter, the accuracy in terms of displacement measurement was about 5.10^{-2} pixels and to the strain calculation was 1.10^{-4}.

To estimate $w^{\bullet}_{\mathrm{def}}$, we used the in-plane displacement field $u=(U,V)$ measured by DIC under the plane stress hypothesis. A method principally based on the integration of the linear momentum equation was used to determine the stress pattern [16-17].

$$\begin{cases} \sigma_{XX}(x,t) = \dfrac{f(t)}{S_0}\exp\left(\varepsilon_{XX}(x,t)\right) \\ \sigma_{XY}(x,y,t) = -\sigma_{XX}(x,t)\dfrac{\partial \varepsilon_{XX}(x,t)}{\partial x}y \\ \sigma_{YY}(x,y,t) = \dfrac{\partial}{\partial x}\left(\dfrac{\sigma_{XX}(x,t)}{2}\dfrac{\partial \varepsilon_{XX}(x,t)}{\partial x}\right).\left(\dfrac{w(x,t)^2}{4} - y^2\right) \end{cases} \tag{7}$$

where σ is the statically admissible stress field, ε the strain field, $f(t)$ the loading force, S_0 the initial cross-section sample and w the sample width.

Finally, we used both stress and strain field measurements to compute the mean volume energy rate corresponding to the mean hysteresis area per block A_{h}. Under the plane stress hypothesis, we computed:

$$f_{\mathrm{L}} A_{\mathrm{h}}(x,y) = \frac{f_{\mathrm{L}}}{N_{\mathrm{c}}}\int_0^{N_c f_L^{-1}} \sigma_{\mathrm{ij}}(x,y,t)\,\dot{\varepsilon}_{\mathrm{ij}}(x,y,t)\,\mathrm{d}t \tag{8}$$

3.2 Estimate of heat sources

The left-hand side of Equation (6) is a differential operator applied to T, while its right-hand side groups all possible heat sources accompanying the deformation process. The regularizing effects of heat diffusion limit the thermal gradients throughout the (small) thickness of the specimen (Figure 1). A depth-wise averaged heat source distribution can thus usually be estimated by using an integrated form over the sample thickness of the heat equation and by assuming that thermal data on the surface remain close to the average temperature [18-20].

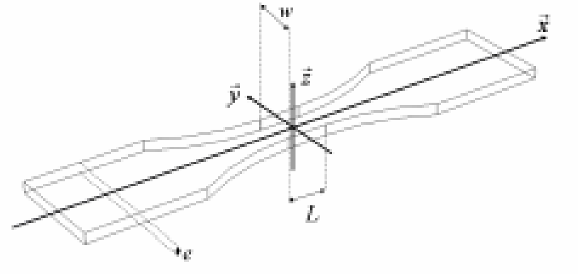

Figure 1: Shape of the specimen

In our experiments, we assumed that the material parameters ρ, *C*, *K* were constant. We considered isotropic heat diffusion and neglected the convective terms in the material time derivative of the temperature. We also assumed that the internal coupling sources remain negligible near thermal equilibrium (i.e. no stress-induced phase change). Besides, we verified that the external heat supply (here limited to radiation exchanges) remained time-independent, so that:

$$-k\Delta T_0 = r_{\text{ext}} \tag{9}$$

where k is the isotropic conduction coefficient and T_0 the equilibrium temperature field of the sample.

For tests performed on thin flat specimens, it was shown in [19] that the temperature measured on surface of the sample remains very close to the depth-wise average temperature as long as the time constant characterizing the heat diffusion remains small compared with the loading time period. Taking all of these hypotheses into account, Eq. (6) could be markedly simplified into a two-dimensional partial derivative equation:

$$\rho C\left(\frac{\partial\overline{\theta}}{\partial t}+\frac{\overline{\theta}}{\tau_{\text{th}}}\right)-k\Delta\overline{\theta}=\overline{d}_1+\overline{s}_{\text{the}} \tag{10}$$

where $\overline{\theta}=\overline{T}-T_0$ is the difference between T and T_0, averaged according to thickness. The symbol τ_{th} stands for a time constant characterizing heat losses perpendicular to the plane of the specimen, while heat conduction in the plane is taken into account by the two-dimensional Laplacian operator.

Construction of the heat source distribution using Eq. (10) requires evaluation of partial derivative operators applied to noisy digital signals. To compute reliable estimates of heat sources, it is then necessary to reduce the noise amplitude without modifying the spatial and temporal thermal gradients. Among several possible methods, a special local least-squares fitting of the thermal signal was considered hereafter (cf. Eq.(13)). Approximation functions account for the underlying heat source spectral properties. Moreover, the linearity of Eq. (10) and that of the respective boundary conditions enabled us to separately analyze the influence of thermoelastic and dissipative heat sources.

Indeed, within the linear thermoelasticity framework, it is easy to verify that:
- the thermoelastic source has the same frequency spectrum as the stress signal;
- the variation of the thermoelastic energy w_{the} vanishes at the end of each loading cycle of period f_{L}^{-1}, so we get:

$$\tilde{w}_{\text{the}} = \int_{f_{\text{L}}^{-1}} s_{\text{the}}\,\mathrm{d}t = 0 \tag{11}$$

Regarding the dissipative effects, we considered dissipation averaged over a whole number n of complete cycles (e.g. n ~ number of cycles per second or per block, etc.):

$$\tilde{d}_1 = \int_{n f_L^{-1}} n^{-1} f_L \, \overline{d}_1 \, dt \tag{12}$$

The new variable $\tilde{d}_1$ may characterize the slow degradation of the material microstructure due to fatigue phenomena including diffuse microplasticity, development of localized persistent slip bands, and progressive damage growth leading to microcracks. The average dissipation per cycle $\tilde{d}_1$ is thus a positive heat source whose spectrum is limited to very low frequencies. With $\tilde{\Delta}s_{\text{the}}$ denoting the thermoelastic source range averaged over n cycles, the aim of the image processing is then to separately assess $\tilde{\Delta}s_{\text{the}}$ and $\tilde{d}_1$.

The local fitting function θ^{fit} of the temperature charts is chosen as:

$$\theta^{\text{fit}}(x,y,t) = p_1(x,y)t + p_2(x,y) + p_3(x,y)\cos(2\pi f_L t) + p_4(x,y)\sin(2\pi f_L t) \tag{13}$$

where the trigonometric time functions describe the periodic part of the thermoelastic effects while the linear time function takes transient effects due to heat loss, dissipative heating and possible drift in the equilibrium temperature into account. Functions $p_i(x,y)$, $i = 1,\dots,4$, are 2^{nd} order polynomials in x and y [20]. These polynomials enabled us to take possible spatial heterogeneity in the source patterns into account. The local approximation zones are rectangular made of (2×6+1) by (2×15+1) pixels. Fitting is also local in time, typically limited to about a hundred frames. A more detailed presentation of the image processing used to determine the heat sources and its check is available in [18-20].

4 EXPERIMENTAL RESULTS

The preliminary results obtained by using both imaging techniques are now presented. DP600 steel produced by Arcelor (dual phase carbon steel) was the material tested. Thin flat specimens were used with a gauge part of 10 mm (length), 10 mm (width) and 2.6 mm (thickness). This material is a hot-rolled steel grade containing ferrite and martensite. **Erreur ! Source du renvoi introuvable.** presents the thermomechanical properties of DP600: the mass density ρ, the heat capacity C, the isotropic heat conduction coefficient k, the linear thermal expansion coefficient α_d, the Young's modulus E, the yield strength $\sigma_{y\,0.2}$, the ultimate strength σ_u and the fatigue limits $\Delta\sigma_\infty$ (obtained at 2×10^6 cycles) expressed in terms of stress range $\Delta\sigma$ for stress ratio $R_\sigma = \sigma_{min}/\sigma_{max}$ equal to -1.

Table 1: Thermomechanical properties of DP600

ρ ($kg.m^{-3}$)	C ($J.kg^{-1}.°C^{-1}$)	k ($W.m^{-1}.°C^{-1}$)	α_d ($10^{-6}.°C^{-1}$)	E (MPa)	$\sigma_{y\,0.2}$ (MPa)	σ_u (MPa)	$\Delta\sigma_\infty$ (MPa) $R_\sigma = -1$
7800	460	64	10-11	213000	400	611	$526 \pm 5^{(*)}$

(*) standard deviation

The tests involved two series of five short loading blocks (N_c=2 400 cycles) performed at increasing $\Delta\sigma$ (180 MPa < $\Delta\sigma$ < 570MPa) with $R_\sigma = -1$ and f_L=30Hz. Between the two series, a block of 100 000 cycles was performed in the maximal stress range. The short blocks were performed to estimate the dissipation levels at different stress amplitudes and at relatively constant damage state. Conversely, the long block at maximal constant stress range aimed at speeding up the fatigue development. The maximal stress range nearly corresponded to the fatigue limit. Note that the visible CCD camera data acquisitions were performed at $f_L=5.55.10^{-3}$ Hz to increase the f_S/f_L ratio, with f_S denoting the sampling frequency, and to improve computation of the energy corresponding to the hysteresis area of the stress-strain curve. The calorimetric analysis showing that the energy dissipated in a cycle was independent of the loading frequency [20], we assumed that the deformation energy corresponding to the hysteresis loop of the stress-strain curve was also rate-independent.

In this paper, energy rate and heat sources are divided by the volume heat capacity ρC of the material to express these latter in $°C.s^{-1}$. This operation makes it possible to define an equivalent heating speed for each type of source and facilitates comparison between the different terms of the energy balance.

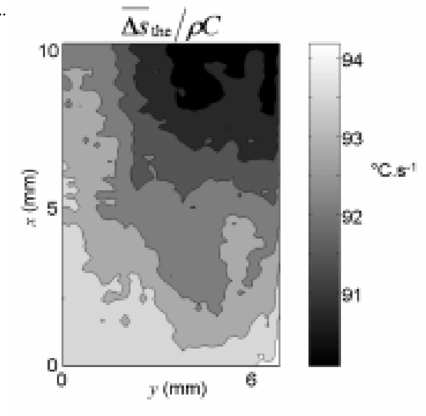

Figure 2: Mean 2D distribution of thermoelastic sources $\tilde{\Delta} s_{\mathrm{the}}(x, y)$ corresponding to the last loading block

In Figure 2, we presented a 2D distribution of the mean thermoelastic source amplitudes averaged over the last loading block. The two main features to be noted are the quite good homogeneity of the coupling source field and the order of magnitude of the thermoelastic effects. The mean $\tilde{\Delta} s_{\mathrm{the}}$ is around 92.5°C.s^{-1} with a standard deviation of about 0.3°C.s^{-1}. Note that the amplitude $\tilde{\Delta} s_{\mathrm{the}}$ is much higher than the dissipation intensity. The energy dissipated per cycle was also compared with the anelastic energy corresponding to the hysteresis loop.

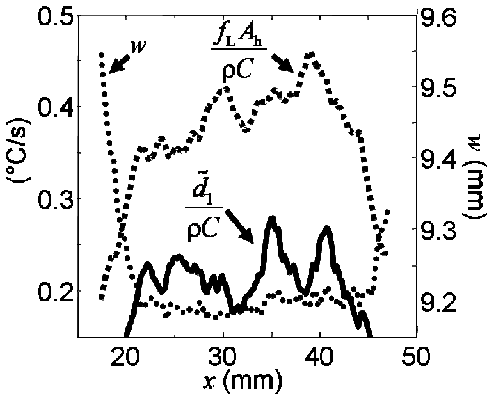

Figure 3: Mean profile over the sample width of $f_{\mathrm{L}} A_{\mathrm{h}}$ and $\tilde{d}_1$.

In Figure 3, the average longitudinal dissipation profile corresponding to the last block can be compared with A_{h}, which is the anelastic energy rate profile. In both cases, we observed that the anelastic work was higher than the energy dissipated in a cycle. We finally plotted the “initial” width variations $w(x)$ of the specimen to show the reader the limits of the gauge part and the sample geometry. Here, by “initial” we mean prior to the observed block.

In Figure 4, the energy balance was performed for all blocks by considering the mean anelastic energy and dissipated energy values over the sample gauge part.

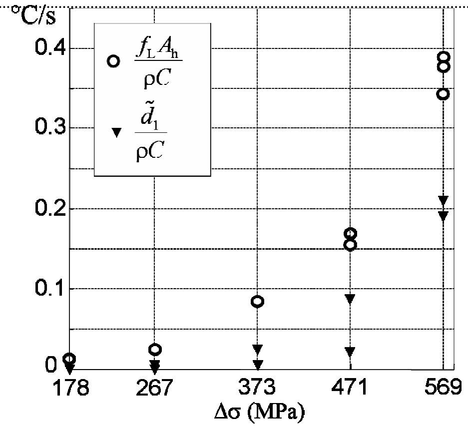

Figure 4: Mean $f_\mathrm{L} A_\mathrm{h}$ and $\tilde{d}_1$ values over the gauge part and per block

5 COMMENTS

This result deserves some comment since the hysteresis area is often identified with the dissipated energy. By combining equations (1) and (5), we get the following expression of the volume deformation energy rate:

$$\sigma : \dot{\varepsilon} = \rho\dot{e} + d_1 - \rho T\dot{s} = \rho\dot{e} + d_1 - \rho C\dot{T} + s_\mathrm{the} + s_\mathrm{ic} \tag{14}$$

Integrating Equation (14) over a mechanical cycle leads to the hysteresis area A_h. If the mechanical cycle is also a thermodynamic cycle, the hysteresis area can come from intrinsic dissipation and/or thermomechanical coupling sources [21]. Concerning DP600 steel fatigue, we found that the variation in the thermoelastic energy w_the vanished at the end of each loading cycle. Besides we neglected the internal coupling sources. The hysteresis area is thus due to internal energy and dissipated energy variations as soon as a periodic oscillation of the temperature is reached (generally obtained after some hundreds of cycles). We then interpreted the difference between the energy of the hysteresis loop and the dissipated energy as an internal energy variation due to irreversible fatigue mechanisms:

$$\int_0^{N_C f_\mathrm{L}^{-1}} \rho C\dot{T}\,\mathrm{d}t = 0 \Rightarrow f_\mathrm{L} A_\mathrm{h} = \int_0^{N_C f_\mathrm{L}^{-1}} \rho\dot{e}\,\mathrm{d}t + \tilde{d}_1 \tag{15}$$

At this level we ought to mention the works of Kaleta [12] which showed similar results at the macroscopic scale (i.e. the scale of the specimen). Indeed, in the case of ferritic-perlitic steel, he observed stored energy ratios associated with the stress-strain hysteresis loop varying from 37.4% for low cycle fatigue tests (LCF), and up to 67.3% for high cycle fatigue tests (HCF).

6 CONCLUSION

In this paper, we presented a combined application of DIC and IRT to the fatigue of DP 600 steel. We used kinematic and thermal data to estimate the deformation energy rate, thermoelastic source amplitude and mean intrinsic dissipation per cycle. The deformation energy rate distribution was computed using strain field measurements, with the stress estimated using a method based on the integration of the linear momentum equation. The heat source distributions were derived from thermal data using a local expression of the heat equation. The linearity of the diffusion equation and that of the boundary conditions allowed us to estimate the sources separately. Finally, the preliminary results obtained on DP 600 steel were presented. They showed that the amounts of deformation energy corresponding to the stress-strain hysteresis loop were systematically greater than the dissipated energy per cycle. A thermodynamic analysis led us to interpret these differences as internal energy variations. Dissipation and stored energy data will now be used to propose state and evolution equations to describe the kinetics of the fatigue progress.

Acknowledgments

The authors would like to thank Arcelor Research SA and Nippon Steel Corporation for their technical and financial support during this study.

7 REFERENCES

1. H. F. Moore and J. B. Kommers, *Chemical and Metallurgical Engineering*, 1921, 25, 1141–1144
2. Luong, M. P, *Mech. of Mat.*, 1998, 28,155-163.
3. G. La Rosa and A. Risitano, *Int. J. of Fatigue*, 2002, **22**, 1, 65-73.
4. D. Dengel et H. Harig, *Fatigue & Fracture of Engineering Materials & Structures*, 1980, 3(1), 113
5. Krapez, J.C. and Pacou, D., *Proc. of SPIE Thermosense XXIV*, Orlando, 2002, 4710, 435-449.
6. A. Galtier, Contribution à l'étude de l'endommagement des aciers sous sollicitations uni ou multiaxiale., PhD Thesis, ENSAM Bodeaux, 1993.
7. P. Cugy and A. Galtier *Proc. 8th Int. Fatigue Conference*, Stockholm, 2002, 549-556
8. Mabru, C. and Chrysochoos, A. (2001) Dissipation et couplages accompagnant la fatigue des matériaux métalliques. *Proc. Photomécanique' 01*, Poitiers, 375-382
9. G. I. Taylor and M. A. Quinney, *Proc. of the Royal Society, London*, A143, 1933, 307-326
10. O. W. Dillon, *Int. J. of Solids and Structures*, 2(2), 1966, 181-204
11. R. Harry, F. Joubert and A. Gomaa , *J. of Engineering Materials and Technology*, Transactions of the ASME, 1981, 103(1), 71-76
12. J. Kaleta *4th Int. Conf. on Low Cycle Fatigue and Elasto-Plastic Behaviour of Materials*, Garmisch-Partenkirchen, Germany, 7-11 September, 1998, 93-98
13. B. Nayroles, R. Bouc, H. Caumon and J. C. Chezeaux. *Int. J. of Engineering Science*, 1981, 19, 929-947
14. B. Wattrisse, A. Chrysochoos, J.-M. Muracciole and M. Nemoz-Gaillard, , *J. of Exp. Mech.*, 2000, 41, n° 1, 29-38
15. P Germain, Q. S. Nguyen, and P. Suquet, *J. of Applied Mechanics*, 1983, 50, 1010-1020
16. B. Wattrisse, A. Chrysochoos, J.-M. Muracciole and Nemoz-Gaillard, M. *European J. of Mech., A/ solids*, 2001, 20, 189-211
17. A. Chrysochoos, J.-M. Muracciole, and B. Wattrisse, *Proc. of Symposium on Continuous Damage and Fracture*; Cachan, France, 2000, 41-51
18. A. Chrysochoos, and H. Louche, *Int. J. of Engng Sci.*, 2000, 38, 1759-1788
19. T. Boulanger, A. Chrysochoos, C. Mabru and A. Galtier, *Int. J. of Fatigue*, 2004, 26**,** 221-229
20. B. Berthel, B. Wattrisse, A. Chrysochoos and A. Galtier, *Strain: an int. J. for Exp. Mech.*, 2007, 43(3), 273-279
21. R. Peyroux, A. Chrysochoos, C. Licht and M. Löbel, *Int. J. of Engineering Science*, 1998, 36(4), 489-509